Insulator–metal transition and ultrafast crystallization of $Ga_{40}Sb_{60}/Sn_{15}Sb_{85}$ multiple interfacial nanocomposite films

Xuan Guo, Yifeng Hu, Qingqian Chou & Tianshu Lai

Journal of Materials Science: Materials in Electronics

ISSN 0957-4522
Volume 30
Number 21

J Mater Sci: Mater Electron (2019)
30:19302-19308
DOI 10.1007/s10854-019-02290-0

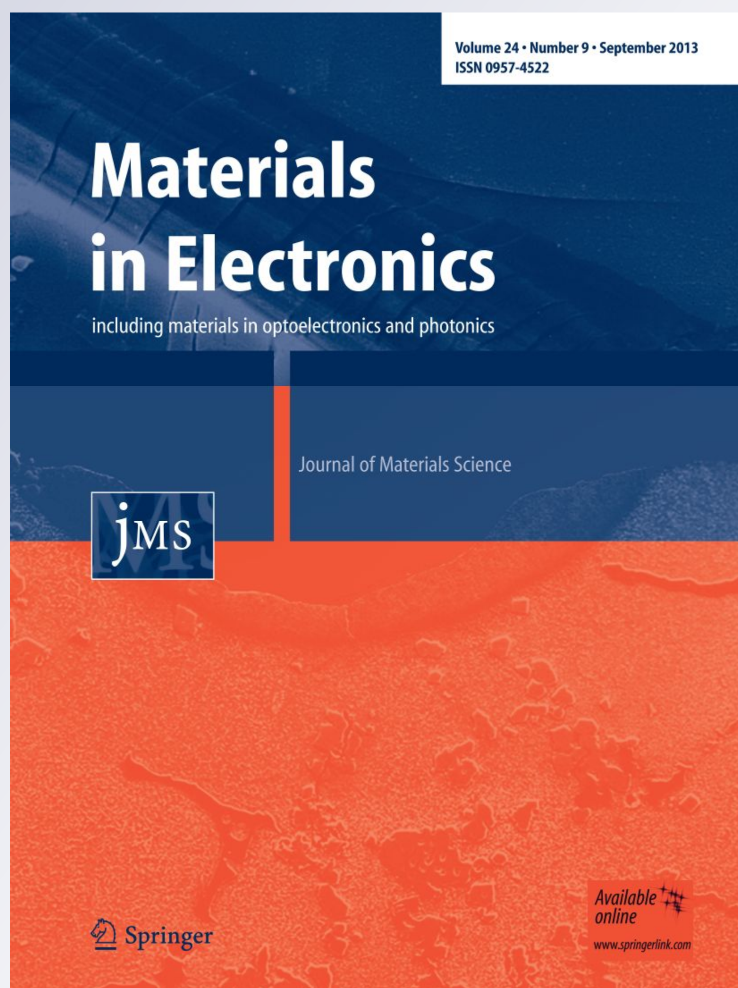

Springer

Your article is protected by copyright and all rights are held exclusively by Springer Science+Business Media, LLC, part of Springer Nature. This e-offprint is for personal use only and shall not be self-archived in electronic repositories. If you wish to self-archive your article, please use the accepted manuscript version for posting on your own website. You may further deposit the accepted manuscript version in any repository, provided it is only made publicly available 12 months after official publication or later and provided acknowledgement is given to the original source of publication and a link is inserted to the published article on Springer's website. The link must be accompanied by the following text: "The final publication is available at link.springer.com".

Springer

Author's personal copy

Journal of Materials Science: Materials in Electronics (2019) 30:19302–19308
https://doi.org/10.1007/s10854-019-02290-0

Insulator–metal transition and ultrafast crystallization of $Ga_{40}Sb_{60}$/$Sn_{15}Sb_{85}$ multiple interfacial nanocomposite films

Xuan Guo[1] · Yifeng Hu[1,3,4] · Qingqian Chou[2] · Tianshu Lai[2]

Received: 24 July 2019 / Accepted: 26 September 2019 / Published online: 30 September 2019
© Springer Science+Business Media, LLC, part of Springer Nature 2019

Abstract

The phase change behavior of $Ga_{40}Sb_{60}$/$Sn_{15}Sb_{85}$ multiple interfacial film was studied systematically for its application in phase change memory. The thermal stability of amorphous state was evaluated using the Arrhenius formulas. The evolution of phase structure indicates that the Sb phase exists in the Sb-rich $Ga_{40}Sb_{60}$/$Sn_{15}Sb_{85}$, $Ga_{40}Sb_{60}$ and $Sn_{15}Sb_{85}$ films. The change in density and thickness during crystallization was obtained by X-ray reflectance. The nanoscale change in roughness of the $Ga_{40}Sb_{60}$/$Sn_{15}Sb_{85}$ film was confirmed by atomic force microscopy. The rate for crystallization and amorphization transformation was measured by a picosecond laser pump-probe system. The phase change memory device based on $[Ga_{40}Sb_{60}$ (7 nm)/$Sn_{15}Sb_{85}$ (3 nm)$]_5$ thin film was fabricated. An ultra-fast switching and low power were achieved for $Ga_{40}Sb_{60}$/$Sn_{15}Sb_{85}$ multiple interfacial film.

1 Introduction

As the promising next-generation mainstream storage technology, phase change random access memory (PCRAM) has great advantages in speed as well as storage density compared to flash memory [1]. The storage of the data is based on the reversible phase transition of the chalcogenide compound material induced by an electrical pulse or heating manner. The RESET process can be achieved with a high and short electrical pulse, while the SET one can be obtained in a low but long electrical pulse. The significant difference between the resistivity of two states is used to distinguish the binary logic levels of "0" and "1" [2]. As the core of PCRAM, the performance of phase change materials directly affects the characteristics of devices. Therefore, the phase change material needs to meet the requirements of fast crystallization speed, good thermal stability and low operating power consumption.

With the improvement of phase change materials in recent years, the traditional material $Ge_2Sb_2Te_5$ (GST) has exposed more and more problems, such as the relatively low 10-year data retention temperature (85 °C), resulting in poor thermal stability. This makes it impossible to be applied in the automotive electronics sector (~125 °C) and industrial control aviation (~150 °C) [3]. In addition, GST belongs to a nucleation dominated crystallization mechanism. Its crystallization time is more than 100 ns, which is not comparable with DRAM (10 ns). To this end, we hope to develop a new material that is far superior to GST in terms of speed and power consumption. Zifang He et al. [4] have confirmed that the $SnSb_4$/Ge multiple interfacial film has a rapid crystallization rate. XRD analysis shows that the Sb phase still exists before and after recombination, which can shorten the crystallization time of the material. The GaSb/Sb_2Te_3 film with superlattice structure prepared by Yegang Lu [5] et al. have both good thermal stability and low operating power consumption. When these materials are applied in PCRAM, the crystallization time (SET) is less than 10 ns, and the erasing speed is improved. Based on previous researches, we combined the $Ga_{40}Sb_{60}$ (GS) and $Sn_{15}Sb_{85}$ (SS) materials to obtain a multiple interfacial phase change film

✉ Yifeng Hu
hyf@jsut.edu.cn

✉ Tianshu Lai
stslts@mail.sysu.edu.cn

1 School of Mathematics and Physics, Jiangsu University of Technology, Changzhou 213000, China

2 State-Key Laboratory of Optoelectronic Materials and Technology, School of Physics, Sun Yat-Sen University, Guangzhou 510275, China

3 State Key Laboratory of Silicon Materials, Zhejiang University, Hangzhou 310027, China

4 Key Laboratory of Semiconductor Materials Science, Beijing Key Laboratory of Low Dimensional Semiconductor Materials and Devices, Institute of Semiconductors, Chinese Academy of Sciences, Beijing 100083, China

Author's personal copy

in this work. The reversible phase change and crystallization behavior were investigated in details.

2 Experimental

GS, SS monolayer films and GS/SS multiple interfacial films were prepared by RF magnetron sputtering (single target sputtering and alternating sputtering, respectively). The total thickness of the film was fixed at 50 nm, the deposited substrate was SiO_2/Si (100), and the purity of GS and SS alloy targets were over 99.99 at.%. The substrate temperature was room temperature, and the instrument was cooled by circulating water during sputtering. The background pressure of the vacuum chamber was lower than 1×10^{-4} Pa with a sputtering gas pressure of 0.25 Pa. A low sputtering power of 30 W was adopted to ensure the accurate control of film thickness. The substrate was ultrasonically cleaned prior to use to remove dust, organic and inorganic impurities from the surface. The sample disk kept rotating at a speed of 20 rpm to guarantee the uniformity of films with an argon flow rate of 30 sccm (sccm was standard ML/min).

The *R–T* curves of the phase change films were measured using an in situ resistance–temperature test system to study the phase transition characteristics of the films from amorphous to crystalline state. At the same time, the crystallization activation energy (E_a) of the film was calculated with isothermal crystallization to evaluate its thermal stability. The reflectance of the film was measured by a near-infrared spectrophotometer (NIR, 7100 CRT, XINMAO, China), and the band gap was obtained by Kubelka–Munk's law. The phase structure was analyzed using an X-ray diffractometer (XRD, PANalytical, Netherlands) with Cu target, K ray, scanning angle range of 20°–60° in the scanning speed of 1° $\min^{-1}$. The change of film thickness during crystallization was determined by an X-ray reflectometer (XRR). The surface morphology of the film was observed by atomic force microscopy (AFM, FM Nanoview 1000). The picosecond laser pumping probe system was employed to study the phase transition velocity by irradiating the film with a mode-locked ytterbium-doped yttrium aluminum garnet laser at a wavelength of 532 nm for about 30 ps. The *I–V* and *R–V* curves of the PCRAM device cells based on the GS/SS multiple interfacial film were tested using a Tektronix AWG5012B arbitrary waveform generator and a Keithley 2602 A parameter analyzer.

3 Results and discussion

As shown in Fig. 1, all the films are in a high-resistance state before crystallization. The resistivity increases with the thickness of the GS layer in the GS/SS multilayer phase change films. Higher resistivity means less free electrons participating in conduction. As the temperature rises gradually, the film reaches its crystallization temperature (T_c) [6]. As can be seen from the Fig. 1, the corresponding T_c for SS, [GS (5 nm)/SS (5 nm)]$_5$, [GS (6 nm)/SS (4 nm)]$_5$, [GS (7 nm)/SS (3 nm)]$_5$, GS thin films were 189, 223, 238, 266 and 330 °C, respectively. In general, the higher crystallization temperature reveals that the phase change film has better amorphous thermal stability but higher programming power consumption. Compared with SS, the GS/SS multiple interfacial films have more stable amorphous resistance state. In addition, the value of amorphous resistance for the GS/SS multiple interfacial films significantly increases with more GS, which can reduce the pulse current of the Joule heating and is conducive to reducing the power consumption in the RESET process [7]. The resistivity of the amorphous GS/SS films differs by at least two orders of magnitude from that of the crystalline films, which is suitable for PCRAM application.

In order to further analyze the thermal stability of phase-change films, the isothermal annealing is carried out to evaluate the difficulty of crystallization. The Arrhenius formula is the common model used to quantificationally assess the data retention and can be expressed as [8]:

$$t = t_0 \exp\left(E_a / k_b T\right) \quad (1)$$

where t, τ_0, k_b and T are the failure times, the pre-factor depends on the nature of the material, the Boltzmann constant and the absolute temperature, respectively. Figure 2 is a plot of failure time versus $1/(k_b T)$. The extrapolated temperatures for the 10-year lifetime (T_{10}) of [GS (5 nm)/SS (5 nm)]$_5$, [GS (6 nm)/SS (4 nm)]$_5$ and [GS (7 nm)/SS (3 nm)]$_5$ films are 154, 168 and 179 °C, respectively, which exceed the requirements of automotive electronics industry (120 °C) [9, 10]. From the slope of Fig. 2, the activation energy (E_a) of the GS/SS multiple interfacial film can be

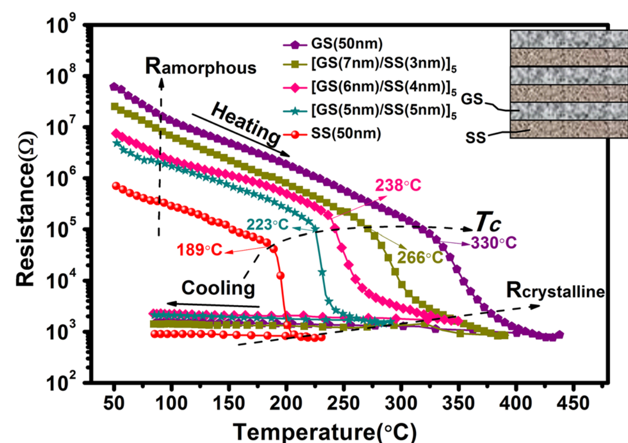

Fig. 1 Resistance as a function of temperature for GS and SS monolayer thin films, GS/SS multiple interfacial films with different thickness ratio at a heating rate of 30 °C/min

Author's personal copy

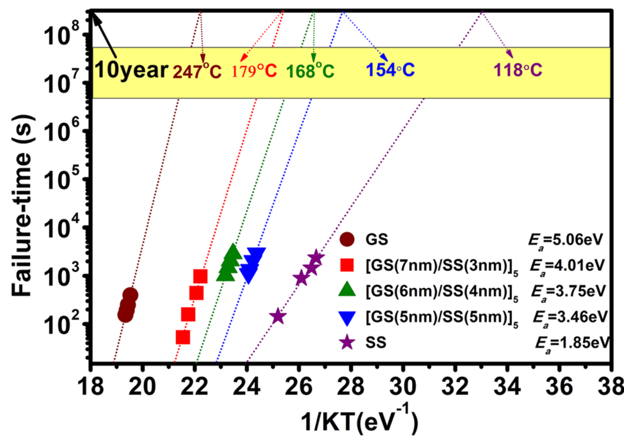

Fig. 2 Plots of failure time versus reciprocal temperature, showing the data retention

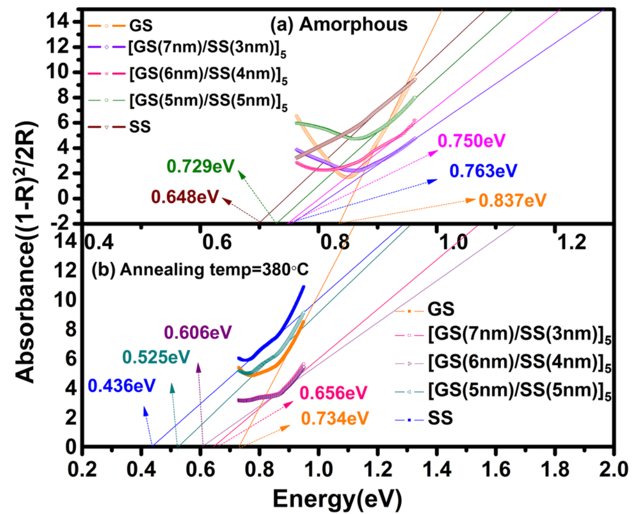

Fig. 3 The Kubelka–Munk function of GS, SS monolayer thin films and GS/SS multiple interfacial films for **a** amorphous and **b** crystalline states

obtained. With the increase of the proportion of GS layer in the GS/SS film, the E_a increased from 3.46 eV of [GS (5 nm)/SS (5 nm)]$_5$ to 4.01 eV of [GS (6 nm)/SS (4 nm)]$_5$. The values are just between the GS (5.06 eV) and SS (1.85 eV) monolayer films. It can be seen that changing the composition thickness in multiple interfacial films can effectively regulate the structural switching barrier in phase transition. The excellent amorphous thermal stability makes the GS/SS films can be used in higher temperature environments [11].

The reflectance spectra of GS/SS films were measured by UV–Vis–NIR spectrophotometry in the wavelength range of 400 to 2500 nm. As shown in Fig. 3, the band gap energy can be determined by extending the absorption edge onto the energy axis, where the conversion of reflectance to absorbance is obtained by the Kubelka–Munk function (K–M) [12]:

$$K/S = (1 - R)^2/(2R) \tag{2}$$

where R, K and S are reflectance, absorption coefficient and scattering coefficient, respectively.

Figure 3 shows that the energy band gaps of amorphous SS, [GS (5 nm)/SS (5 nm)]$_5$, [GS (6 nm)/SS (4 nm)]$_5$, [GS (7 nm)/SS (3 nm)]$_5$ and GS thin films are 0.648, 0.729, 0.750, 0.763 and 0.837 eV, respectively. At 380 °C, the band gaps of crystalline SS, [GS (5 nm)/SS (5 nm)]$_5$, [GS (6 nm)/SS (4 nm)]$_5$, [GS (7 nm)/SS (3 nm)]$_5$ and GS thin films are 0.436, 0.525, 0.606, 0.656 and 0.734 eV, respectively. The value of band gap for the overall crystalline states is smaller than that of the amorphous ones, indicating that the carrier concentration becomes larger. Besides, the energy band gap of the films increases with the thickness of GS layer, which is in accordance with the trend of the R–T curves in Fig. 1 [13]. With a broader band gap, the film needs more energy to accumulate for phase change.

Figure 4 provides the XRD diffraction patterns of the deposited and annealed GS/SS, GS and SS films. In the deposited state (Fig. 4c), no diffraction peaks of all films were observed, indicating an amorphous structure. When the annealing temperature rises to 380 °C above the T_c for all films, the diffraction peaks (012) and (104) belonging to the Sb phase appear in Fig. 4b. It can be concluded that the Sb phase is present in the Sb-rich GS/SS, GS and SS films. In Fig. 4a, no Sb phases are observed for annealed [GS (7 nm)/SS (3 nm)]$_5$ at 220 and 260 °C, which is consistent with the results of Fig. 1. Besides, Sb (104) peak is absent for [GS (7 nm)/SS (3 nm)]$_5$ film, which may be the result of the suppression of multiple interface. It should also be noted that all of the three graphs have diffraction peaks belonging to the Si phase, indicating that Si is derived from the Si substrate [14].

The atomic rearrangement in the phase change process can change the volume or density of the film. The resulted voids are detrimental to the contact between phase change material and the electrode. It can cause the degradation of cycle durability and reliability of the PCRAM device. Figure 5a shows the XRR pattern of the crystalline and amorphous states of the [GS (7 nm)/SS (3 nm)]$_5$ film. It can be found that the incident angle corresponding to the maximum or minimum peak of the crystalline state shifts to a higher angle. The modified Bragg equation is used to determine the density change before and after crystallization [15]:

$$\sin\theta_m = 2\delta + (m + \Delta m)^2\left(\frac{\lambda}{2t}\right)^2 \tag{3}$$

Author's personal copy

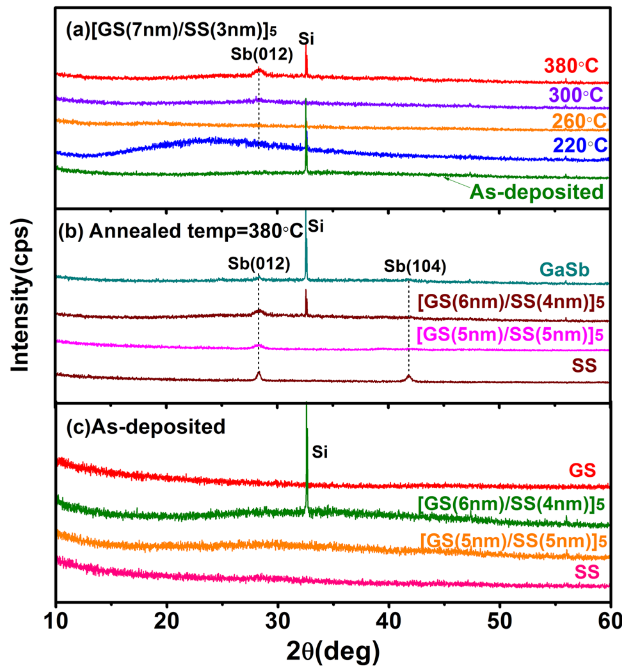

Fig. 4 XRD patterns of **a** [GS (7 nm)/SS (3 nm)]$_5$ thin film annealed at various temperatures for 5 min; **b** GS, SS and GS/SS thin films annealed at 380 °C for 5 min; **c** as-deposited state of GS, SS and GS/SS thin films

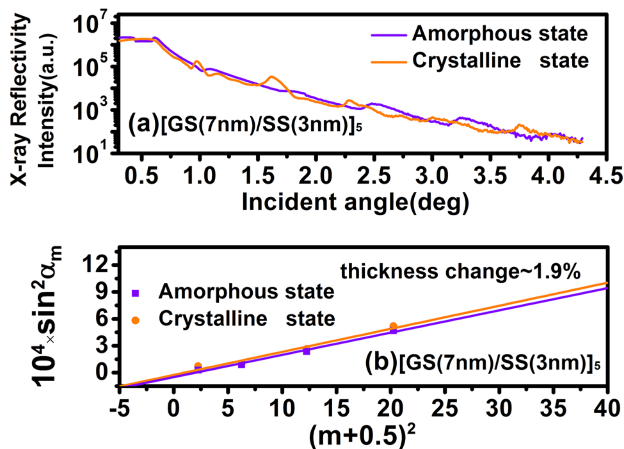

Fig. 5 **a** XRR curves and **b** modified Bragg fitting curves of amorphous and crystalline [GS (7 nm)/SS (3 nm)]$_5$ thin films

where δ is a constant, m in θ_m is the reflection coefficient, λ is the wavelength (0.154 nm), t is the film thickness, m in $m + \Delta m$ is the correction coefficient, and the value of Δm is 0.5, and the value of Δm corresponds to the minimum or maximum value of the XRR diffraction peak for each reflection coefficient. The linear curve of $sin^2\alpha_m$ and $(m + \Delta m)^2$ is shown in Fig. 5b. The relationship between the thickness variation of the film is calculated as [15]:

$$t = \lambda/2\sqrt{k} \tag{4}$$

From this, it is calculated that the thickness change of the [GS (7 nm)/SS (3 nm)]$_5$ film before and after crystallization is 1.9%, which is smaller than the conventional GST (6.8%) film [16]. The existence of multiple interface restrains the phase transition, leading to a smaller volume change. The smaller thickness variation during the phase change can improve the reliability and extend the life of the PCRAM.

The morphology of the film surface also changes accompanied by the internal stress. Figure 6 shows the AFM images of the GS and GS/SS films before and after crystallization. As can be clearly seen in Fig. 6a–d, all film surfaces appear flat and smooth with a small Root-Mean-Square (RMS) roughness of [GS (7 nm)/SS (3 nm)]$_5$ = 1.078 nm, [GS (6 nm)/SS (4 nm)]$_5$ = 1.127 nm, [GS (5 nm)/SS (5 nm)]$_5$ = 1.143 nm and GS = 1.193 nm. After annealing at 380 °C for 10 min in Ar atmosphere, many small and dense grains can be observed, indicating the amorphous to crystalline phase transition. Accordingly, the value of RMS increases a little to 1.078 = 1.193 nm. Compared with GS, the grain quantity of GS/SS multiple interfacial films is much less and the surface roughness is lower. It should be the results of the inhibitory effect of interface clamping. This research reveals that the PCRAM device based on GS/SS multiple interfacial films can have a better contact between the phase-change layer and electrode, which can improve the fatigue durability [17].

For PCRAM, the speed of reading and writing data is crucial. Picosecond laser technology is used to study the speed of phase switching. It is well known that amorphous states exhibit high electrical resistance and low reflectivity, while the crystalline states have low electrical resistance and high reflectivity [18]. Figure 7a, c, e are the transitions from amorphous to crystalline state. The crystallization time for GS, [GS (7 nm)/SS (3 nm)]$_5$ and SS are 7.0, 6.1 and 5.8 ns, respectively. Usually the crystallization process takes more time than the amorphization one, and the reverse phase change requires higher laser pulse energy. As shown in Fig. 7b, d, f, the amorphization time for GS, [GS (7 nm)/SS (3 nm)]$_5$ and SS are 4.7, 4.3 and 3.9 ns, respectively. [GS (7 nm)/SS (3 nm)]$_5$ film has a shorter crystallization and amorphization time than GS, which is also faster than GST (17.7 and 16.5 ns) [19]. The reasons may be that the low thermal conductivity of the composite multilayer structure hinders the heat diffusion to increase heating efficiency and reduce heating time. Besides, the rich Sb atoms with a weak Sb-Sb bond can act as a nucleation center. A large number

Author's personal copy

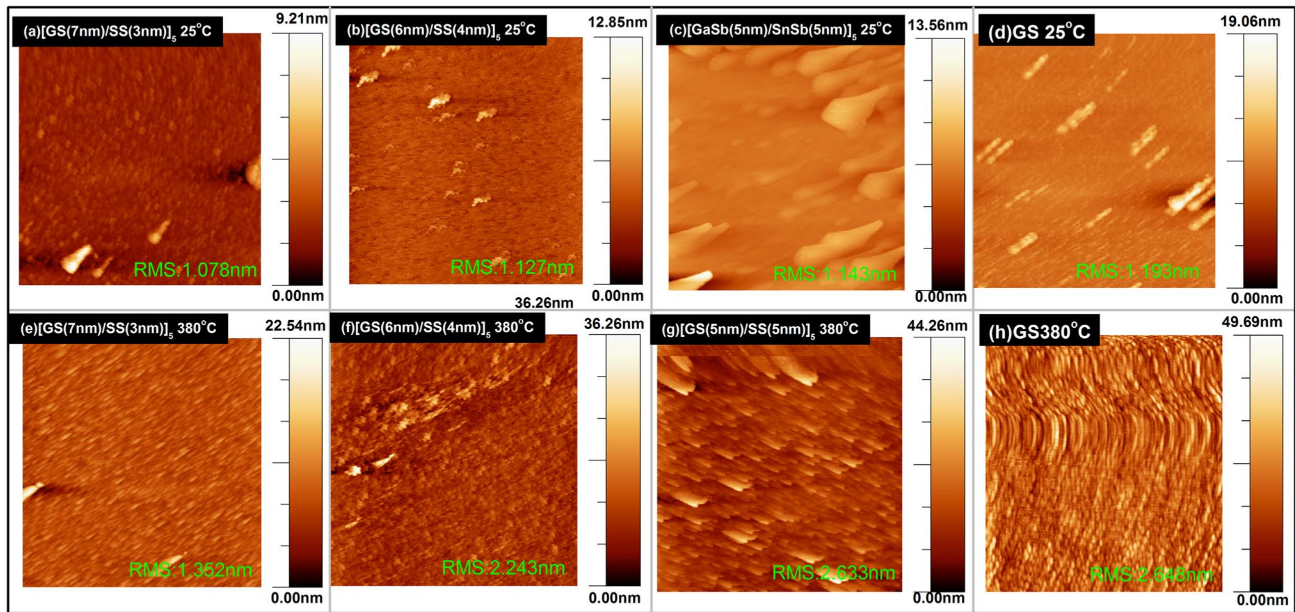

Fig. 6 AFM images for as-deposited and annealed films **a**, **e** [GS (7 nm)/SS (3 nm)]$_5$; **b**, **f** [GS (6 nm)/SS (4 nm)]$_5$; **c**, **g** [GS (5 nm)/SS (5 nm)]$_5$; **d**, **h** GS

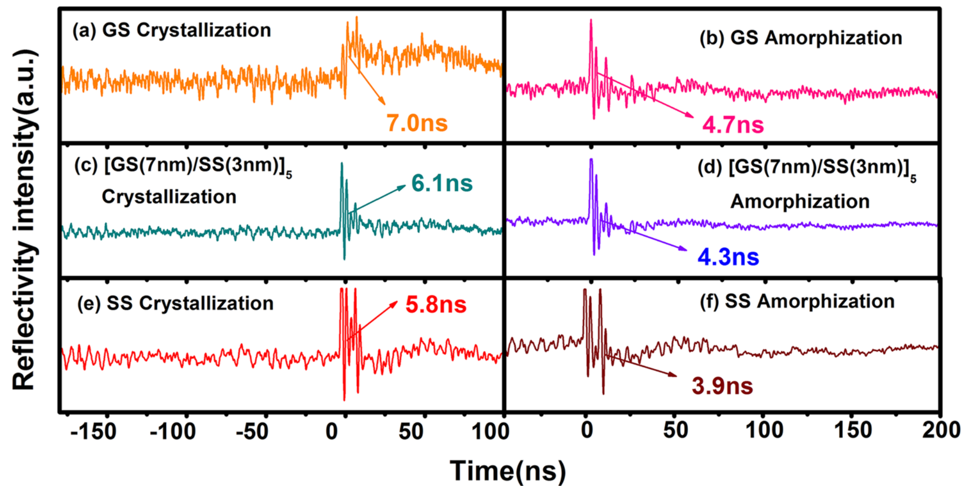

Fig. 7 Reversible reflectivity evolution of the GS, [GS (7 nm)/SS (3 nm)]$_5$ and SS thin films induced by consecutive picosecond laser pulses with different fluencies: **a**, **c**, **e** crystallization process; **b**, **d**, **f** amorphization process

of crystal nuclei can promote the crystallization process and shorten the crystallization time [20].

PCRAM device cells based on [GS (7 nm)/SS (3 nm)]$_5$ and GST thin films were fabricated using a 0.18 μm CMOS process technology to test and verify the electrical performance. A schematic of the cross-sectional structure is shown in the inset of Fig. 8a. The role of TiN is to increase the adhesion of (top electrode) TE and (phase change layer) PCL. Figure 8a shows the current–voltage (*I*–*V*) curves for the SET operation, which corresponds to the phase transition from the high resistance to low resistance state. The threshold voltage (V_{th}=2.1 *V*) of [GS (7 nm)/SS (3 nm)]$_5$ film is smaller than GST (V_{th}=4.2 *V*), indicating that the power consumption of the multiple interfacial film during the SET process is smaller [21]. From the resistance–voltage (*R*–*V*) characteristic curves in Fig. 8b, the reversible phase transition can be achieved by a pulse of 200 ns for the [GS (7 nm)/SS (3 nm)]$_5$ film, indicating that it has a faster switching speed than GST (500 ns). In addition, the RESET voltage (2.70 V) for [GS (7 nm)/SS (3 nm)]$_5$ film is smaller than

Author's personal copy

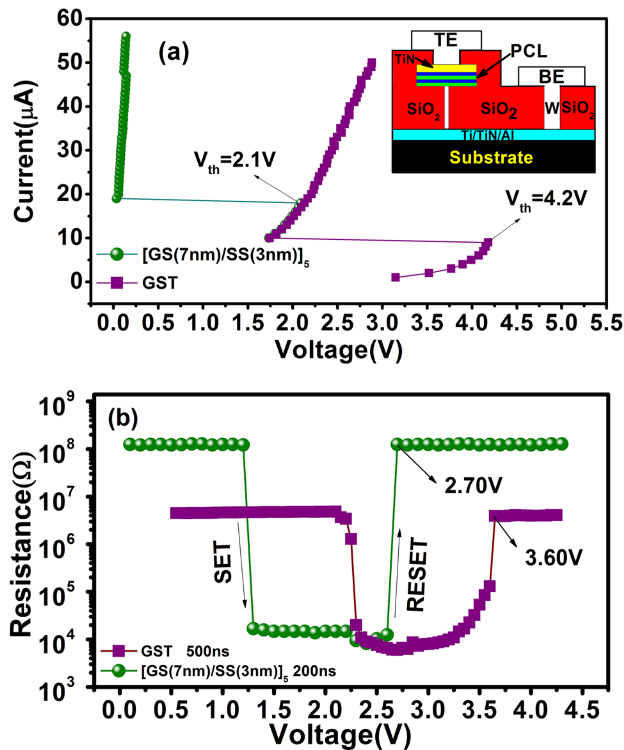

Fig. 8 **a** *I–V* and **b** *R–V* curves of the PCRAM cells based on [GS (7 nm)/SS (3 nm)]$_5$ and GST thin films. The inset in **a** shows the schematic diagram of the PCRAM cell structure

GST (3.60 V), which reveals that the RESET power consumption of the multiple interfacial film is lower [22].

4 Conclusions

The reversible phase change and crystallization behavior of GS/SS multiple interfacial film were investigated. The comparison shows that the T_c increased from 189 °C of SS to 266 °C of [GS (7 nm)/SS (3 nm)]$_5$. And the data retention temperature increased from 118 to 179 °C for 10 years. At the same time, GS/SS multiple interfacial films have higher E_a compared with SS. The band gap value of the crystalline composite film was smaller than that of the amorphous state, resulting in a larger carrier concentration. The Sb phase was present in the Sb-rich GS/SS films. The [GS (7 nm)/SS (3 nm)]$_5$ film had a smaller thickness change (1.9%) and roughness change before and after crystallization. The crystallization and amorphization time for [GS (7 nm)/SS (3 nm)]$_5$ are 6.1 and 4.3 ns, respectively. Based on the [GS (7 nm)/SS (3 nm)]$_5$ thin film, the V_{th} in RESET process is 2.7 V. The results showed that GS/SS multiple interfacial film was a promising phase change material with fast-speed and low-power in PCRAM application.

Acknowledgements This work was supported by National Natural Science Foundation of China (Grant Nos. 11974008 and 11774438) and Changzhou key laboratory of high technology research (Grant No. CM20173002) and sponsored by Qing Lan Project and the Opening Project of State Key Laboratory of Silicon Materials (Grant No. SKL2017-04) and the Opening Project of State Key Laboratory of Silicon Materials (Grant No. SKL2017-04) and the Opening Project of Institute of Semiconductors, Chinese Academy of Sciences(Grant No. KLSMS-1805) and Practice Innovation Program of Jiangsu Province (Grant No. SJCX18_1024).

References

1. W.H. Wu, Z.F. He, S.Y. Chen, J.W. Zhai, S.N. Song, Z.T. Song, Investigation on the crystallization properties and structure of oxygen-doped Ge_8Sb_{92} phase change thin films. J. Appl. Phys. **9**, 095602 (2017)
2. S.Y. Chen, W.H. Wu, J.W. Zhai, S.N. Song, Z.T. Song, Sb_7Te_3/ZnSb multilayer thin films for high thermal stability and long data retention phase-change memory. Mater. Sci. Eng. B **218**, 59–63 (2017)
3. H.P. You, Y.F. Hu, X.Q. Zhu, H. Zou, S.N. Song, Z.T. Song, Investigation of Cu–Sn–Se material for high-speed phase-change memory applications. J. Mater. Sci.-Mater. Electron. **28**, 10199–10204 (2017)
4. Z.F. He, P.Z. Wu, R.R. Liu, J.W. Zhai, T.S. Lai, S.N. Song, Z.T. Song, Superlattice-like $SnSb_4$/Ge thin films for ultra-high speed phase change memory applications. CrystEngComm **7**, 1230–1234 (2016)
5. Y.G. Lu, S.M. Li, S.N. Song, Z.T. Song, B. Liu, T. Wen, T.S. Lai, Study on the crystallization process of GaSb-Sb2Te3 pseudobinary films for phase-change random access memory. J. Nanosci. Nanotechnol. **13**, 976–979 (2013)
6. Z.G. Li, Y.G. Lu, M. Wang, X. Shen, X.H. Zhang, S.N. Song, Z.T. Song, Controllable multilevel resistance state of superlattice-like GaSb/Ge_2Te films for ultralong retention phase-change memory. J. Non-Cryst. Solids **481**, 110–115 (2018)
7. W.H. Wu, S.Y. Chen, J.W. Zhai, X.Y. Liu, T.S. Lai, S.N. Song, Z.T. Song, Multi-level storage and ultra-high speed of superlattice-like $Ge_{50}Te_{50}$/Ge_8Sb_{92} thin film for phase-change memory application. Nanotechnology **40**, 405206 (2017)
8. X.Q. Zhu, R. Zhang, Y.F. Hu, T.S. Lai, J.H. Zhang, H. Zou, Z.T. Song, Crystallization process of superlattice-like Sb/SiO_2 thin films for phase change memory application. Chin. Phys. Lett. **5**, 056803 (2018)
9. L.L. Shen, S.S. Song, Z.T. Song, L. Li, T.Q. Guo, Y. Cheng, L.C. Wu, B. Liu, S.L. Feng, Properties of Ti–Sb–Te doped with SbSe alloy for application in nonvolatile phase change memory. J. Mater. Sci. **1**, 923–927 (2017)
10. P. Singh, P. Sharma, V. Sharma, A. Thakur, Linear and non-linear optical properties of Ag-doped $Ge_2Sb_2Te_5$ thin films estimated by single transmission spectra. Semicond. Sci. Technol. **32**, 4 (2017)
11. K. Ren, R.H. Li, J.B. Shen, T.J. Xin, S.L. Lv, Z.G. Ji, Z.T. Song, Study on the phase change behavior of nitrogen doped Bi_2Te_3 films. J. Alloys Compd. **754**, 227–231 (2018)
12. H. Zou, Y.F. Hu, X.Q. Zhu, Z.T. Song, Simultaneously high thermal stability and ultra-fast phase change speed based on samarium-doped antimony thin films. RSC Adv. **7**, 31110–31114 (2017)
13. P.I. Kuznetsov, E.S. Shchamkhalova, V.O. Yapaskurt, V.D. Shcherbakov, V.A. Luzanov, G.G. Yakushcheva, V.A. Jitov, V.E. Sizov, MOVPE deposition of Sb_2Te_3 and other phases of Sb-Te system on sapphire substrate. J. Cryst. Growth **471**, 1–7 (2017)

Author's personal copy

14. Zhou Xl, J.K. Behera, L.V. Shilong, L.C. Wu, Z.T. Song, R.E. Simpson, Avalanche atomic switching in strain engineered Sb_2Te_3-GeTe interfacial phase-change memory cells. Nano Futures **1**, 025003 (2017)
15. H.P. You, Y.F. Hu, X.Q. Zhu, H. Zou, S.N. Song, Z.T. Song, Simultaneous ultra-long data retention and low power based on $Ge_{10}Sb_{90}/SiO_2$ multilayer thin films. Appl. Phys. A **124**, 168 (2018)
16. C.Z. Wang, J.W. Zhai, S.N. Song, Z.T. Song, M.C. Sun, B. Shen, Investigation of GeTe/Ge2Sb2Te5 nanocomposite multilayer films for phase-change memory applications. Electrochem. Solid-State Lett. **14**, H258–H260 (2011)
17. Y.F. Hu, H.P. You, X.Q. Zhu, H. Zou, J.H. Zhang, S.N. Song, Z.T. Song, Superlattice-like GeTe/Sb thin film for ultra-high speed phase change memory applications. J. Non-Cryst. Solids **457**, 141–144 (2017)
18. W.L. Zhu, T. Wen, Y.F. Hu, X.Y. Liu, D. Gu, T.S. Lai, J.W. Zhai, Cycle number manipulating effect on crystallization temperature of superlattice-like [Ge/Ge8Sb92]n phase-change films. J. Alloys Compd. **723**, 936–941 (2017)
19. Y.F. Hu, H. Zou, L. Yuan, J.Z. Xue, Y.X. Sui, W.H. Wu, J.H. Zhang, X.Q. Zhu, S.N. Song, Z.T. Song, Improved phase change behavior of Sb_2Se material by Si addition for phase change memory. Scr. Mater. **115**, 19–23 (2016)
20. Wu PZ, Hu YF, Wen T, Liu XY, Lai TS, Zhai JW. Exploring mechanism on nano-structuring manipulation of crystallization temperature of superlattice-like $[GeSb/Ge]_3$ phase-change films. in 2016 International Workshop on Information Data Storage and Tenth International Symposium on Optical Storage, USA: SPIE; 2016
21. Y.F. Hu, X.Q. Zhu, H. Zou, H.P. You, L.J. Zhai, S.N. Song, Z.T. Song, Nanosecond switching in superlattice-like GeTe/Sb thin film for high speed and low power phase change memory application. ECS J. Solid State Sci. Technol. **6**, 45–48 (2017)
22. H. Zou, X.S. Wang, Y.F. Hu, X.Q. Zhu, Y.X. Sui, D.H. Shen, Z.T. Song, Optical thermometry based on the upconversion luminescence from Er doped $Bi_7Ti_4TaO_{21}$ ferroelectric ceramics. J. Mater. Sci. **26**, 6502–6505 (2015)

Publisher's Note Springer Nature remains neutral with regard to jurisdictional claims in published maps and institutional affiliations.